2021 Sixteenth International Conference on Ecological Vehicles and Renewable Energies (EVER)

Performance Comparison of Offline and Real-Time Models of a Power Take-Off for Qualification Activities of Wave Energy Converters

Luca Castellini
UMBRAGROUP s.p.a.
06034 Foligno (PG), Italy
Email: lcastellini@umbragroup.com

Federico Gallorini and Giacomo Alessandri
VGA s.r.l., 06053 Deruta (PG), Italy
Emails: federico.gallorini@vgasrl.com,
giacomo.alessandri@vgasrl.com

Erick Alves and Dan Montoya
Department of Electric Power Engineering
Norwegian University of Science and Technology (NTNU)
7034 Trondheim, Norway
Emails: erick.f.alves@ntnu.no,
dan.montoya@ntnu.no

Elisabetta Tedeschi
Department of Electric Power Engineering, NTNU
7034 Trondheim, Norway
Department of Industrial Engineering
University of Trento, 38123 Trento, Italy
Email: elisabetta.tedeschi@ntnu.no

***Abstract*—A Power Take-Off (PTO) is responsible to convert wave to electrical power and is one of the core sub-systems of any Wave Energy Converter (WEC). As result, assessing the PTO performance is one of the key aspects of the WEC design and, looking at the optimization of all WEC subsystems, it directly impacts the LCOE assessment and the commercialization of the technology. To address this need, it is crucial to approach WEC modeling with the awareness of the different techniques. The paper presents part of the results of the IMAGINE R&D program developed with the support of European Union's H2020 research and innovation programme. This project is aimed at the design and test of a novel PTO drive intended for a range of WEC configurations. In particular, the paper presents a complete simulation platform, which allows realistic simulations of the performance of a 250 kW modular electro-mechanical generator (EMG) when coupled to an oscillating wave surge converter (OWSC) device. This model is compared to a corresponding simplified model more suitable for real-time (RT) hardware-in-the-loop (HIL) testing. A comparison between the two is provided as fundamental check to guarantee that the simulated environment is as similar as possible to the real-space and hence to validate the product maturity even though with a certain level of simplification.**

***Keywords*—wave energy; wave energy conversion; systems modelling; power take-off; ballscrew; electric generator; test bench.**

I. Introduction

While the world moves towards a radical energy transition and Europe has set the ambitious target of carbon neutrality by 2050 [1], there is a renewed urge for innovative and efficient ways of generating, transmitting and saving energy. Within this context, ocean energy can play a crucial role in the transition towards a more sustainable society, with a target of $40\,\mathrm{GW}$ of installed power by 2050 [2].

On one hand, wave energy has a tremendous potential at global level and is one of the most promising forms of ocean energy. On the other hand, developing a wave energy converter (WEC) is still a complex and evolving subject. The abundance of design concepts, the variability of input loads, the harsh marine environment, high installation and maintenance costs are some of the aspects that prevented wave energy to reach a technical and commercial maturity comparable to other renewable energy technologies [3], [4], [5].

Among the subsystems in a WEC, power take-offs (PTOs) are of primary significance. They are critical to define aspects such as reliability, survivability, controllability and maintainability and have a direct impact on the energy yield of the overall device [3], [4], [5]. Not least, PTOs may account for up to $22\,\%$ of the costs in a typical wave energy project [6].

Recently, a modular PTO system developed by UMBRAGROUP based on an a novel electrical machine that converts slow-speed, reciprocating linear motion into electric power with high efficiency and reliability was introduced [7] and experimentally validated [8]. Also, the modular nature of this PTO system was explored during

the selection and early-design phases of a WEC [9], [10] under the Innovative Method for Affordable Generation IN ocean Energy (IMAGINE) project within the European Union's Horizon 2020 research and innovation programme.

Considering how important the PTO is in a WEC, its testing and integration with other key subsystems shall be pursued from an early design phase. Typically, these tasks are achieved through simulation of wave-to-wire models [11]. Moreover, the hardware-in-the-loop (HIL) testing scheme is considered as a state-of-the-art tool to bridge the gap between the laboratory and the real operational environment in several industries, such as automotive, aerospace and power systems. In the wave energy sector, HIL testing has already been used for different PTO concepts [12], [13], [14], [15], [16], [17].

To assess the expected performance of a WEC employing the UMBRAGROUP PTO system, this paper presents two alternative wave-to-wire modeling approaches. The first is an offline model including an oscillating wave surge converter (OWSC) device, the modular PTO system based on parallel electro-mechanical units (EMUs), the power converters and all controllers and functionalities required to operate a WEC safely, reliably and efficiently. The second model is a simplified and faster version of the first, which is suitable for real-time (RT) HIL testing.

The main goals of this work are: 1) describing these two models; 2) comparing their results; 3) highlighting their advantages, drawbacks, and for which purposes they are adequate during the WEC project cycle.

II. Background

The IMAGINE project aims at designing, manufacturing and testing a novel linear generator to decrease the cost of current PTO technologies, while increasing their efficiency and reliability. The core element of the electro-mechanical generator (EMG) is a ballscrew: a load-carrying mechanical component where the balls convert the slow-speed linear motion of the input shaft into a high-speed rotary motion of the nut and vice-versa. Ballscrews have typically high efficiencies, thanks to the rolling friction between balls and threads. At the same time, permanent magnets integrated in the nut allow to produce a magnetic rotating field, coupled to an externally mounted stator. With this arrangement, the screw pitch (i.e. the axial distance between adjacent threads) and the number of poles of the rotor act respectively as mechanical and magnetic gears, increasing the frequency of the induced voltage.

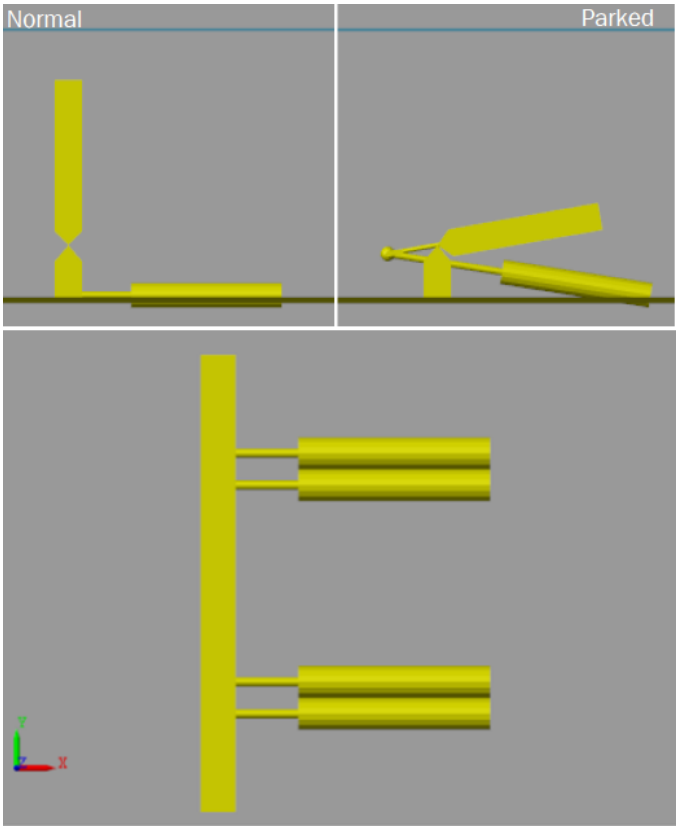

Fig. 1. Views with rest and extended PTO conditions of the IMAGINE OWSC model (IMAGINE project, 2018).

In the context of the IMAGINE project, the target of designing a 250 kW modular EMG started by identifying the loading envelope that the generator would be subject to. Within this task, three different WECs types and three deployment sites were evaluated [9]. The selection process concluded with the identification of the OWSC concept as the preferred reference model for estimation of the detailed EMG input data. The choice was primarily related to the capability of its architecture to constrain the stroke under different working conditions. Given the available energy at the selected deployment sites, a scaling exercise was conducted to have a WEC hosting a PTO system consisting of four 250 kW peak power EMGs in parallel. Further, the deployment of modular units was performed; each EMG would be composed of two EMUs working in unison. This arrangement has been selected by UMBRAGROUP to provide redundancy and to demonstrate the capability of the modular EMG to work in parallel. Fig. 1 provides an overview of the EMGs along the WEC width and of the kinematics linking the EMGs and the OWSC flap.

Then, generic load cases such as power production, occurrence of faults, start-up and parking were analyzed to identify the overall EMG loading envelope. Starting from a pure damping control law, where the damping

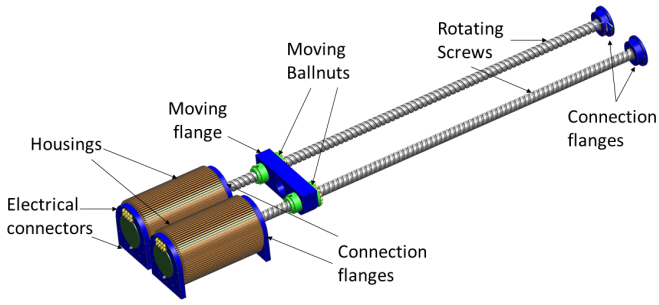

Fig. 2. EMG design (IMAGINE project, 2019).

variable was identified with an optimization procedure, force and power limits have been integrated to allow the EMG working within its operative conditions (165 kN and 250 kW respectively). While the power limit was a constraint of the IMAGINE project, the force limit was set by UMBRAGROUP, according to a preliminary design of the ballscrew. From the numerical simulation results, maximum values have been extracted to define the overall loading envelope. The final EMG design contains two EMUs with moving ballnuts and rotating screws, connected to the same moving flange. At one end, the screw is connected to the rotor of a permanent magnet synchronous machine (PMSM). On the other end, a support with a roller bearing allows to withstand the screw weight while allowing its rotation. Fig. 2 provides an overview the EMG main components.

According to the EMG design, VGA designed a test rig by connecting an EMG and an EMU to the same carriage. This approach, agreed with UMBRAGROUP, would allow to test the EMG both as generator and actuator, thanks to the reversibility of ballscrew and PMSM technologies. When using the EMG as a generator, the EMU would exert a load on the EMG moving flange. Tests under this configuration would allow the demonstration of the EMG modularity by using more EMUs in parallel. In the case of the EMG working as an actuator, the EMU would be tested up to its maximum operating limits, demonstrating the coherence with the input design data. Fig. 3 provides an overview of the test rig layout.

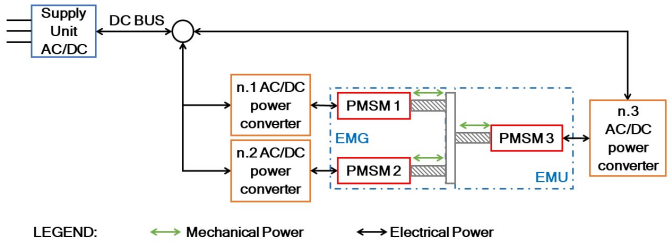

Fig. 3. IMAGINE Test rig layout (IMAGINE project, 2020).

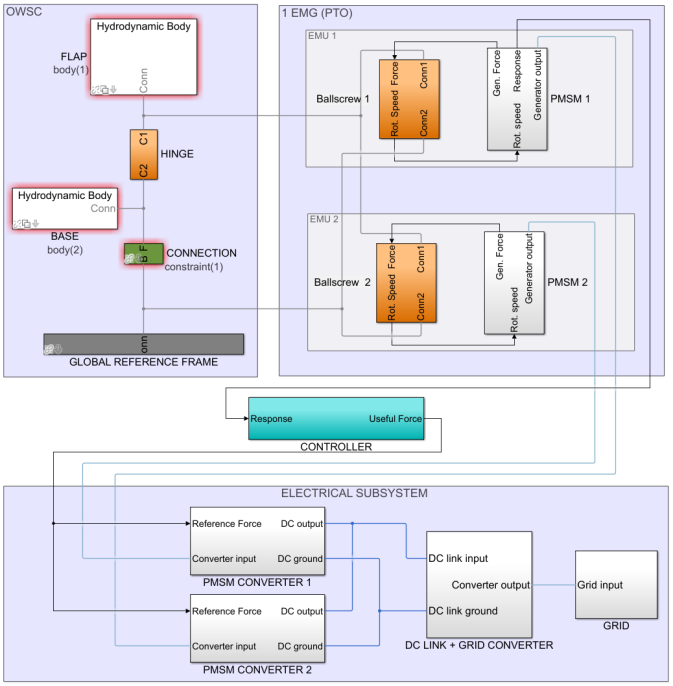

Fig. 4. Offline Matlab/Simulink Model including the WEC, PTO, Control and Electrical Subsystems.

III. Offline Model

The performance of the described PTO was evaluated by a detailed wave-to-wire model developed by NTNU integrating the following subsystems: the OWSC device, the PTO system based on parallel EMUs, the power converters, the controllers and electrical components. The simulation model, shown in Fig. 4, has been developed in Matlab/Simulink v2018a using the WEC-Sim [18] toolbox v3.0 and the Simscape Power Systems 6.9 library.

The hydrodynamic model of the OWSC WEC is formed by the *Flap*, *Hinge*, *Base*, *Fixed connection*, and *Seabed* blocks.

The EMG is formed by two EMUs, each composed of a ballscrew and a PMSM. The input to each *Ballscrew* block is the applied force coming from the PMSM and the output is the angular speed of the PMSM.

The *PMSM* block models the electrical generator in detail. The output is the PMSM force connected to the *Ballscrew* block and its input is the angular speed from the ballscrew. An additional port, containing the PMSM stator variables, is connected to the *PMSM converter* block. The latter represents the average model of a 2-level, three-phase voltage source converter (VSC) using sinusoidal pulse width modulation (SPWM).

All power converters share the same DC link. The model has two input/output ports: the DC port of the converter, that is connected to other power converter

TABLE I. PARAMETERS OF THE OFFLINE MODEL BLOCKS

Flap		
Width 14.3 m	Thickness 1.1 m	Height 6.6 m
Base		
Width 14.3 m	Thickness 1.1 m	Height 2.2 m
Seabed	**Hinge**	**Ballscrew**
Water depth 10.8 m	Height from seabed 2.2 m	Pitch 60 mm
PMSM		
V_{max} 690 V_{rms}	p 20 pairs	ψ_{pm} 0.235 Wb
I_{max} 185.2 A_{rms}	L_d 1.003 mH	L_q 1.203 mH
Generator Converter		
V_{ac} 690 V_{rms}	2-level VSC with SPWM	V_{dc} 1000 V
Grid Converter		
V_{ac} 400 V_{rms}	2-level VSC with SPWM	V_{dc} 1000 V
DC Link	**Grid**	
Capacit. 100 mF	Series Induct. 0.102 mH	Freq. 50 Hz

DC ports, and the three-phase port, that is connected to the three-phase port of the *PMSM* block. The reference signal to control the converter comes from the *controller* block and is connected to another input of the *PMSM converter* block.

The *DC link + grid-side converter* block models the DC link and the grid converter. The grid-side converter is a 2-level, three-phase VSC converter that uses SPWM. It is modeled using average technique. In addition, it has two input/output ports. The first one is the DC link port, and the second one is the three-phase port that goes to the grid.

The *Grid* block models the transformer and the grid. There is one input/output three-phase port that is connected to the *DC link + grid converter* block.

The *Controller* block is a high-level controller that implements a control strategy on the PTO force to maximize power production. This way, the controller gives an EMU force reference which is then converted in a PMSM reference torque (current) on each generator converter block. In order to set the optimum EMU reference force, the controller considers as inputs the position, speed and acceleration signals that are measured on the EMG and, as it was commented above, the output of the controller is the EMU reference force that goes to the *PMSM converter* block.

For the rest of this paper, the variables $\psi_{pm}, I_s^*, i_d^*, i_q^*, I_{max}, V_{max}, L_d, L_q, \omega_e, p$ refer to the permanent magnet flux linkage, stator total current, d- and q-axis reference currents, stator maximum current and voltage, total inductance in the d- and q-axis, electrical angular speed, and number of pole pairs of the PMSM.

A. MTPA and FW

The PTO reference force is converted into a PMSM reference torque (T^*) which becomes I_s^* inside each generator power converter block. Then, a low-level controller adjusts this reference to satisfy the I_{max}, V_{max} constraints applying both maximum torque per ampere (MTPA) and field weakening (FW) techniques [19], [20]. To set i_d^*, i_q^* using MTPA, the nonlinear equation system formed by eqs. (1), (2) and (3) is solved.

$$T^* = \frac{3}{2}p(\psi_{pm}i_q^* + (L_d - L_q)i_q^* i_d^*) \tag{1}$$

$$i_d^* = \frac{\psi_{pm} - \sqrt{\psi_{pm}^2 + 8(L_q - L_d)^2 I_s^{*2}}}{4(L_q - L_d)} \tag{2}$$

$$i_q^* = sign(I_s^*)\sqrt{I_s^{*2} - i_d^{*2}} \tag{3}$$

The FW technique satisfies the V_{max} limit of the PMSM [21]. For that, the generator power converter block solves the fourth degree polynomial seen in eq. 4 to readjust i_q^*.

$$A_4 i_q^{*4} + A_3 i_q^{*3} + A_2 i_q^{*2} + A_1 i_q^* + A_0 = 0 \tag{4}$$

where

$$\begin{aligned} A_4 &= 9p^2(L_d - L_q)^2 L_q^2 \omega_e^2 \\ A_3 &= 0 \\ A_2 &= 9p^2\psi_{pm}^2 L_q^2 \omega_e^2 - 9p^2(L_d - L_q)^2 V_{max}^2 \\ A_1 &= -12T^* p \psi_{pm} L_d L_q \omega_e^2 \\ A_0 &= 4T^{*2} L_d^2 \psi_{pm}^2 \end{aligned}$$

Finally, eq. 5 obtains the readjusted FW i_d^*.

$$i_d^* = -\frac{\psi_{pm}}{L_d} + \frac{1}{L_d}\sqrt{\left(\frac{V_{max}}{\omega_e}\right)^2 - L_q^2 i_q^{*2}} \tag{5}$$

IV. REAL-TIME MODEL

The RT HIL model was derived by NTNU and VGA from the offline version presented in section III. This variant was developed to: 1) check the feasibility of running the offline model in a RT platform; 2) be integrated in the test rig described in section II for the EMG qualification tests under the IMAGINE project.

The RT model is divided into two subsystems: 1) *SC_GUI*, integrating all elements required for the supervision and control of the test rig; 2) *SM_PLANT*, including all the dynamic models required for RT simulation. Fig. 5 provides an overview of the latter.

The *wecSim model* block integrates the OWSC model and the kinematics of the PTO. It receives the torque applied by each EMU and calculates the equilibrium between PTOs and hydrodynamic loads defining the position, speed, and acceleration at the EMG axis.

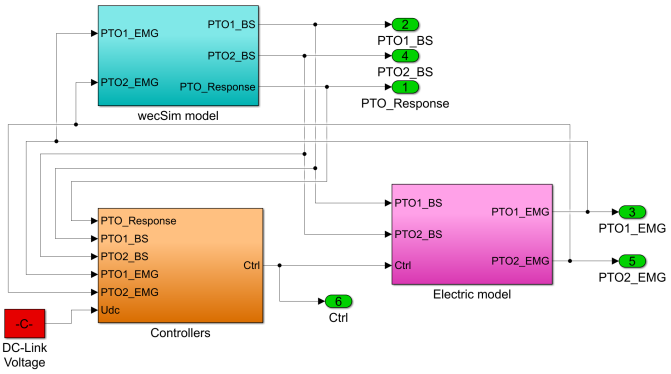

Fig. 5. Components of the *SM_PLANT* subsystem

The *Controllers* block is organized in two different levels. First, a high-level controller that implements an adaptive PTO control strategy defines the reference torque that the EMU should apply to produce a certain force at the input axis and maximize the WEC power extraction. Then, a low-level controller defines the three-phase voltage to be applied at the PMSM for achieving the reference torque.

The *Electric model* block simulates the PMSM dynamics that, according to the input three-phase voltages and EMG rotor speed, defines the corresponding currents and thus the output torque exerted by each EMU.

To implement FW and MTPA concurrently in the *Controllers* block as described in section III-A, it is necessary to solve a nonlinear system of equations and a fourth degree polynomial for every simulation step. This task demands a reasonable amount of processing power and it is not suitable for real-time embedded systems. Therefore, a near-optimal implementation of the FW and MTPA problems was developed to achieve RT performance. This solution is inspired in [20], [22] and presented in the following algorithm:

$$i_{d,MTPA} = \frac{\psi_{pm} - \sqrt{\psi_{pm}^2 + 8(L_q - L_d)^2 I_s^{*2}}}{4(L_q - L_d)}$$
$$i_{d,MTPA} = max(i_{d,MTPA}; -I_{max})$$
$$i_{q,MTPA} = sign(I_s)\sqrt{I_s^{*2} - i_{d,MTPA}^2}$$
$$\omega_{base} = \frac{V_{max}}{\sqrt{(L_d i_{d,MTPA} + \psi_{pm})^2 + (L_q i_{q,MTPA})}}$$
IF $|\omega_e| \leq \omega_{base}$
$$i_d^* = i_{d,MTPA}$$
$$i_q^* = i_{q,MTPA}$$
ELSE
$$aux = (L_d^2 - L_q^2)(\psi_{pm}^2 + (L_q I_s^*)^2 - (\frac{V_{max}}{\omega_e})^2)$$
$$i_{d,FW} = \frac{-\psi_{pm} L_d - \sqrt{(\psi_{pm} L_d)^2 - aux}}{(L_d^2 - L_q^2)}$$
$$i_d^* = max(i_{d,MTPA}; -I_{max})$$
$$i_q^* = \sqrt{I_s^{*2} - (i_d^*)^2}$$
$$T_{FW} = \frac{3}{2} p i_q^* (\psi_{pm} + (L_d - L_q) i_d^*)$$
IF $T_{FW} \geq T^*$
$$i_q^* = \frac{T^*}{T_{FW}} i_q^*$$
ENDIF
ENDIF

V. Case Study

To compare the fidelity of the RT and offline models, the WEC was simulated in several operational conditions for a total of 900 s. Table II presents results for two representative sea states of a target site off the south west coast of England (coordinates 49.8N 5.8W). These are the sea states with the highest mean annual energy production ($T_p = 7\,\text{s}, H_s = 2.25\,\text{m}$) and forces ($T_p = 8\,\text{s}, H_s = 5.25\,\text{m}$).

The normalized root mean-squared error (NRMSE) was used as metric to quantitatively compare the models:

$$NRMSE(x_{RT}, x_{off}) = 1 - \sqrt{\frac{\sum_{n=1}^{N}(x_{RT} - x_{off})^2}{\bar{x}_{off}}} \quad (6)$$

where N is the number of samples for the entire simulation and x_{RT}, x_{off} are the values of the RT and offline models respectively. The proposed metric compares two models without accounting for the error sign and is a measure of accuracy [23]. Its values vary between $-\infty$ (bad fit) and 1 (perfect fit).

The results from table II reveal that the RT model can reproduce the dynamics of the offline model with fidelity. However, discrepancies on force, reference and output torque are present. When investigating the results closer, two main sources for deviations are found: 1) the discretization of control loops in the RT model; 2) the different field weakening strategies in the two models.

The first source causes overshoot of the current controllers due to additional delay introduced by the discretization of integrators. This effect is well-documented in the control systems literature, such as in [24], and better visualized in fig. 6a. The overshoot is more prominent in sea states with lower H_s because the EMG current and torque controllers operate without saturation for longer periods. As consequence, the NRMSE values of the PTO force, EMG measured and reference torques

TABLE II. COMPARISON BETWEEN OFFLINE AND REAL-TIME MODELS

Variable	$\mathbf{T_p = 7\,s}$ $\mathbf{H_s = 2.25\,m}$	$\mathbf{T_p = 8\,s}$ $\mathbf{H_s = 5.25\,m}$
PTO position	0.976	0.998
PTO velocity	0.982	0.998
PTO acceleration	0.968	0.996
PTO force	*0.873*	0.971
EMG measured torque	*0.859*	0.967
EMG reference torque	*0.848*	0.988
EMG mechanical power	0.965	0.920
EMG electrical power	0.945	0.901

are reduced in these sea states. To obtain the offline model performance, the current controllers in the RT model shall be re-tuned considering the delays introduced by discretization. For a HIL setup, measurement and communication delays must also be considered.

The second source of discrepancy is better visualized in fig. 6b. In sea states with higher H_s, the velocity goes above the EMG rated speed often, and hence the FW algorithm is activated more frequently. By comparing the EMG current behavior between the models, one will notice that the reduction of the absolute value of i_q and increase of i_d during FW is sharper in the RT model. This happens because the RT implementation is near-optimal and prioritizes keeping voltage and current limits of the PMSM within allowed limits.

All in all, the RT model was regarded as a valuable tool for the EMG qualification tests of IMAGINE. It allows testing the modular PTO system developed by UMBRAGROUP in very realistic simulation conditions but under the RT constraints of VGA's HIL test rig.

Not least, the RT model can be used for other purposes in a WEC design cycle using UMBRAGROUP's modular PTO concept. For instance, a better evaluation of a WEC performance is achieved when specifying physical constraints for each component [11]. The RT model faster performance (up to 10 times faster than the offline model) may allow including these constraints in the initial assessment of a target site where several sea states must be simulated to evaluate important design variables such as the energy yield, peak stroke, velocity, acceleration, forces and power.

On the other hand, it is important to keep in mind the RT model limitations. Peak PTO force may be slightly overestimated in sea states with lower H_s, while average power may be slightly underestimated in sea states with higher H_s. For a detailed evaluation of a specific sea state, including the WEC performance during faults, the use of the offline model is highly recommended.

VI. CONCLUSION

A. Summary of key findings

This paper summarizes the key findings related to the wave-to-wire models of an OWSC device connected to a PTO system, made of parallel EMUs. First, an offline, detailed model of the overall system was created in Matlab Simulink environment. The wave-flap interaction, its kinematics and interface with the PTO have been modeled through the use of the WEC-Sim toolbox. A block accounting for the mechanical and electrical aspects of the parallelized EMUs has been included. A high-level controller and an electrical subsystem that includes power converters and a DC link have been modeled. Maximum torque per ampere and field weakening techniques have been also included in a low-level controller to adjust the electrical inputs to the PMSMs, according to the torque reference from the high-level controller. Then, a Real-Time Hardware-In-the-Loop model was derived from the detailed model, to allow its execution on a RT platform, in view of the EMG qualification tests. The simplification included the implementation of near-optimal MTPA and FW algorithms.

A comparison between the two models is presented considering the NRMSE as a quantitative metric; the results show that the dynamics of the offline model are well represented by the RT model with execution times up to 10 times faster. However, differences on force, reference and output torques are present. These are mainly due to: 1) the discretization of control loops that introduce additional delays on the adjustment of the current; 2) the balance between i_d^*, i_q^* when the FW algorithm is applied. Both effects influence the torque and force values exerted on the PMSM and ballscrew.

B. Next steps

In the next steps of the IMAGINE project, the HIL model will be integrated into the test rig software and interfaced with the real EMG, power and control systems. These activities will include the re-tuning of the current controllers to account for the delays introduced by the simplified MTPA algorithm and for communication delays between the different parts of the system. Another aspect that will be evaluated is the use of an optimized FW algorithm, leading to an increased output power. Not least, a comparison of the test results with respect to the output of the two Matlab models is also foreseen.

ACKNOWLEDGMENT

The IMAGINE project received funding from the European Union's Horizon 2020 research and innovation programme under grant agreement number 764066.

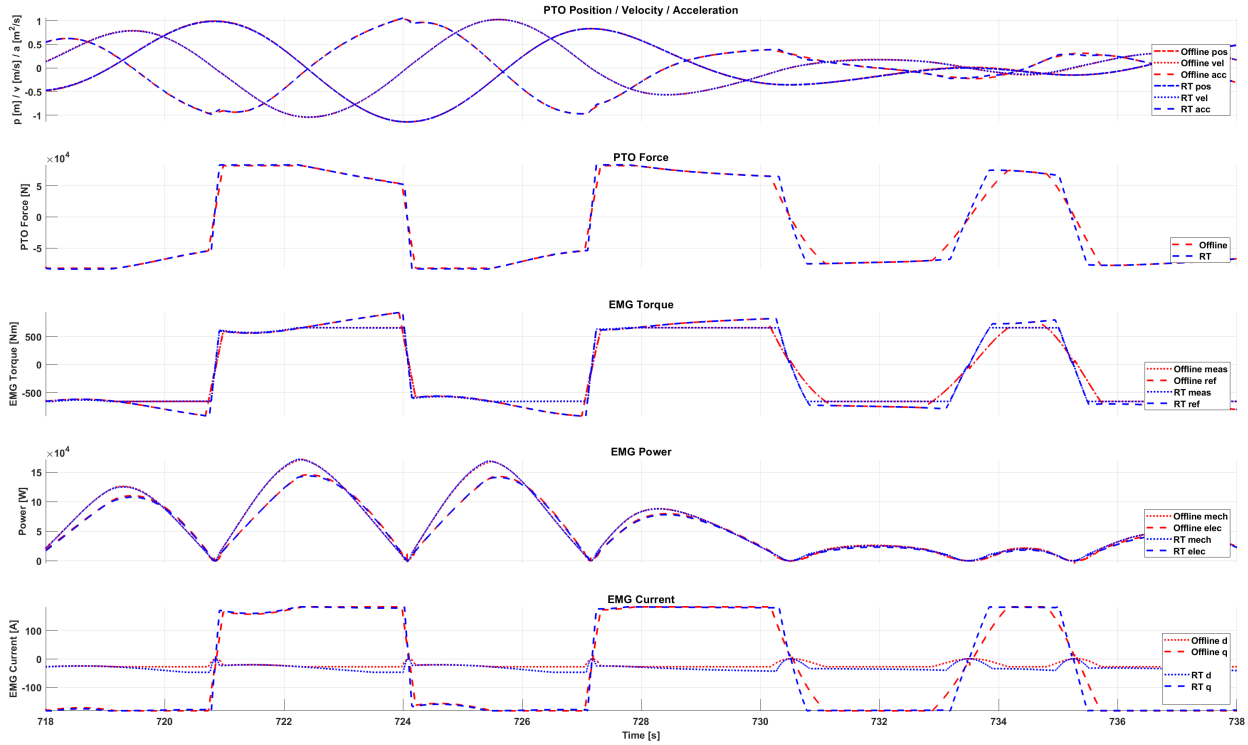

(a)

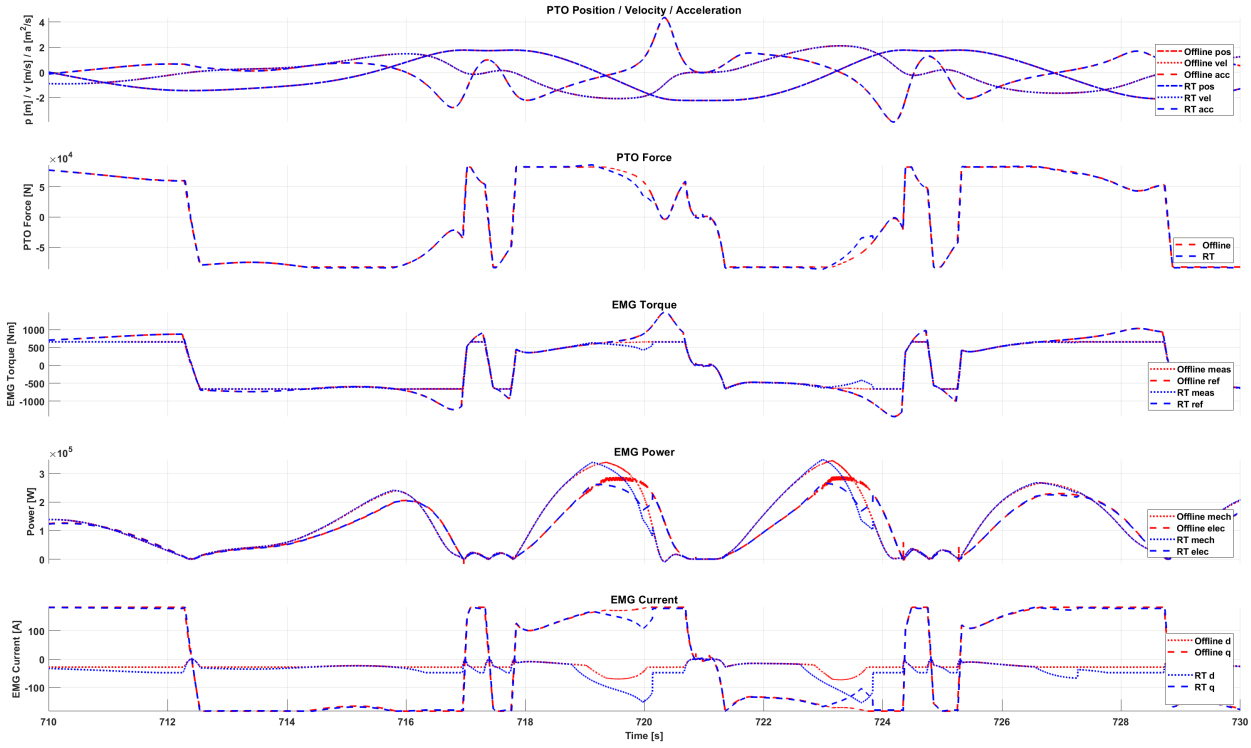

(b)

Fig. 6. Visual comparison between offline and real-time models for two sea states: (a) $T_p = 7\,\mathrm{s}, H_s = 2.25\,\mathrm{m}$; (b) $T_p = 8\,\mathrm{s}, H_s = 5.25\,\mathrm{m}$.

REFERENCES

[1] European Commission, "Committing to climate-neutrality by 2050: Commission proposes European Climate Law and consults on the European Climate Pact," Mar. 2020. [Online]. Available: https://ec.europa.eu/commission/presscorner/detail/en/ip_20_335

[2] ——, "An EU Strategy to harness the potential of offshore renewable energy for a climate neutral future," European Commission, Brussels, Belgium, Communication COM(2020) 741 final, Nov. 2020. [Online]. Available: https://ec.europa.eu/energy/sites/ener/files/offshore_renewable_energy_strategy.pdf

[3] Ocean Energy Forum, "Ocean Energy Strategic Roadmap 2016: Building ocean energy for Europe," Nov. 2016. [Online]. Available: https://webgate.ec.europa.eu/maritimeforum/en/node/3962

[4] TP Ocean, "Strategic Research Agenda for Ocean Energy," Nov. 2016. [Online]. Available: https://www.oceanenergy-europe.eu/wp-content/uploads/2017/03/TPOcean-Strategic_Research_Agenda_Nov2016.pdf

[5] ETIP Ocean, "Strategic Research and Innovation Agenda for Ocean Energy," May 2020. [Online]. Available: https://www.oceanenergy-europe.eu/wp-content/uploads/2020/05/ETIP-Ocean-SRIA.pdf

[6] Carbon Trust, "Accelerating marine energy," Carbon Trust, UK, Tech. Rep. CTC797, Jul. 2011. [Online]. Available: https://prod-drupal-files.storage.googleapis.com/documents/resource/public/Accelerating%20marine%20energy%20-%20REPORT.pdf

[7] L. Castellini, M. D'Andrea, and N. Borgarelli, "Analysis and design of a recipracating linear generator for a PTO," in *2014 International Symposium on Power Electronics, Electrical Drives, Automation and Motion*. Ischia, Italy: IEEE, Jun. 2014, pp. 1373–1379.

[8] L. Castellini, M. D'Andrea, M. Martini, G. Alessandri, D. Coiro, F. De Luca, G. Calise, G. Troise, and A. Vogler, "Experimental tests on a wave-to-wire pivoted system for wave energy exploitation," in *2017 6th International Conference on Clean Electrical Power (ICCEP)*. Santa Margherita Ligure, Italy: IEEE, Jun. 2017, pp. 479–487.

[9] J. Cruz, M. Atcheson, T. Martins, L. Castellini, and M. Martini, "Preliminary load assessment: Umbra's 250 kW EMG Power Take-Off," *Proceedings of the European Wave and Tidal Energy Conference 2019*, no. 1, Sep. 2019.

[10] J. Scriven, J. Cruz, and M. Atcheson, "Upscaling wave energy converters: Size vs. modularity," *Proceedings of the International Conference on Renewable Energies Offshore 2020*, Oct. 2020.

[11] M. Penalba and J. Ringwood, "A Review of Wave-to-Wire Models for Wave Energy Converters," *Energies*, vol. 9, no. 7, p. 506, Jun. 2016.

[12] J. Henriques, R. Gomes, L. Gato, A. Falcão, E. Robles, and S. Ceballos, "Testing and control of a power take-off system for an oscillating-water-column wave energy converter," *Renewable Energy*, vol. 85, pp. 714–724, Jan. 2016.

[13] H. Pedersen, R. Hansen, A. Hansen, T. Andersen, and M. Bech, "Design of full scale wave simulator for testing Power Take Off systems for wave energy converters," *International Journal of Marine Energy*, vol. 13, pp. 130–156, Apr. 2016.

[14] M. Penalba, N. Sell, A. Hillis, and J. Ringwood, "Validating a Wave-to-Wire Model for a Wave Energy Converter—Part I: The Hydraulic Transmission System," *Energies*, vol. 10, no. 7, p. 977, Jul. 2017.

[15] M. Penalba, J.-A. Cortajarena, and J. Ringwood, "Validating a Wave-to-Wire Model for a Wave Energy Converter—Part II: The Electrical System," *Energies*, vol. 10, no. 7, p. 1002, Jul. 2017.

[16] T. D. Dang, C. B. Phan, and K. K. Ahn, "Modeling and Experimental Investigation on Performance of a Wave Energy Converter with Mechanical Power Take-Off," *Int. J. of Precis. Eng. and Manuf.-Green Tech.*, vol. 6, no. 4, pp. 751–768, Aug. 2019.

[17] N. Delmonte, E. Robles, P. Cova, F. Giuliani, F. X. Faÿ, J. Lopez, P. Ruol, and L. Martinelli, "An Iterative Refining Approach to Design the Control of Wave Energy Converters with Numerical Modeling and Scaled HIL Testing," *Energies*, vol. 13, no. 10, p. 2508, May 2020.

[18] Y.-H. Yu, K. Ruehl, J. V. Rij, N. Tom, D. Forbush, D. Ogden, A. Keester, and J. Leon, "Wec-sim v4.2," Dec. 2020. [Online]. Available: https://doi.org/10.5281/zenodo.3924764

[19] J. Sjolte, C. Sandvik, E. Tedeschi, and M. Molinas, "Exploring the Potential for Increased Production from the Wave Energy Converter Lifesaver by Reactive Control," *Energies*, vol. 6, no. 8, pp. 3706–3733, Jul. 2013.

[20] M. Li, "Flux-Weakening Control for Permanent-Magnet Synchronous Motors Based on Z-Source Inverters," Master, Marquette, Milwaukee, WI, Dec. 2014.

[21] C.-T. Pan and J.-H. Liaw, "A Robust Field-Weakening Control Strategy for Surface-Mounted Permanent-Magnet Motor Drives," *IEEE Trans. On Energy Conversion*, vol. 20, no. 4, pp. 701–709, Dec. 2005.

[22] S. Lim, "Sensorless-FOC With Flux-Weakening and MTPA for IPMSM Motor Drives," Texas Instruments, Tech. Rep. SPRACF3, 2018. [Online]. Available: https://www.ti.com/lit/an/spracf3/spracf3.pdf

[23] C. Lewis-Beck and M. Lewis-Beck, *Applied Regression: An Introduction*. 2455 Teller Road, Thousand Oaks California 91320: SAGE Publications, Inc, 2016.

[24] G. F. Franklin, J. D. Powell, and A. Emami-Naeini, *Feedback Control of Dynamic Systems*, 6th ed. Upper Saddle River, NJ: Pearson, 2010.